HHS Public Access

Author manuscript

Biochim Biophys Acta Gen Subj. Author manuscript; available in PMC 2023 December 01.

Published in final edited form as:

Biochim Biophys Acta Gen Subj. 2022 December ; 1866(12): 130238. doi:10.1016/j.bbagen.2022.130238.

Extracellular matrix stiffness regulates degradation of MST2 via SCF $^{\beta TrCP}$

Ana Paula Zen Petisco Fiore[a,b], **Ana Maria Rodrigues**[a], **Helder Veras Ribeiro-Filho**[c], **Antonio Carlos Manucci**[a], **Pedro de Freitas Ribeiro**[a], **Mayara Carolinne Silva Botelho**[a], **Christine Vogel**[b], **Paulo Sergio Lopes-de-Oliveira**[c], **Michele Pagano**[d], **Alexandre Bruni-Cardoso**[a,*]

[a]Departamento de Bioquímica, Instituto de Química, Universidade de São Paulo, São Paulo 05508-000, Brazil

[b]Department of Biology, New York University, New York, NY 10003, USA

[c]Laboratório Nacional de Biociências, Centro Nacional de Pesquisa em Energia e Materiais, Campinas 13083-970, Brazil

[d]Department of Biochemistry and Molecular Pharmacology, Howard Hughes Medical Institute, New York University Grossman School of Medicine, New York, NY 10016, USA

Abstract

The Hippo pathway plays central roles in relaying mechanical signals during development and tumorigenesis, but how the proteostasis of the Hippo kinase MST2 is regulated remains unknown. Here, we found that chemical inhibition of proteasomal proteolysis resulted in increased levels of MST2 in human breast epithelial cells. MST2 binds SCF$^{\beta TrCP}$ E3 ubiquitin ligase and silencing βTrCP resulted in MST2 accumulation. Site-directed mutagenesis combined with computational molecular dynamics studies revealed that βTrCP binds MST2 via a non-canonical degradation motif. Additionally, stiffer extracellular matrix, as well as hyperactivation of integrins resulted in enhanced MST2 degradation mediated by integrin-linked kinase (ILK) and actomyosin stress fibers. Our study uncovers the underlying biochemical mechanisms controlling MST2 degradation

*Corresponding author. brunicar@iq.usp.br (A. Bruni-Cardoso).

Author contribution

APZPF planned, performed, analyzed most experiments and co-wrote the manuscript. AMRS performed all the RT-qPCRs and immunoblots in Supplementary Fig. 4. PRF manufactured all hydrogels. ACM generated cDNA constructs and performed the protein stability assay. MCSB cultured the breast cell lines used in the experiments shown in Fig. 2A. CV supervised the ubiquitylation assay and edited the manuscript. HVRF and PSLO performed the molecular dynamics studies. MP co-supervised part of the study and edited the mansucript. AB-C planned experiments, analyzed data, supervised the study and wrote the manuscript.

Declaration of Competing Interest

The authors declare the following financial interests/personal relationships which may be considered as potential competing interests: Michele Pagano reports a relationship with Coho Therapeutics that includes: equity or stocks. Michele Pagano reports a relationship with CullGen that includes: board membership. Michele Pagano reports a relationship with Kymera Therapeutics that includes: board membership. Michele Pagano reports a relationship with SEED Therapeutics that includes: board membership. Michele Pagano reports a relationship with Santi Therapeutics that includes: consulting or advisory.

M.P. is a consultant for and has financial interests in Coho Therapeutics, CullGen, Kymera Therapeutics, and SEED Therapeutics. M.P. is a cofounder of Coho Therapeutics, is on the SAB of CullGen and Kymera Therapeutics, and is a consultant for Santi Therapeutics. The other authors declare no competing interests.

Appendix A. Supplementary data

Supplementary data to this article can be found online at https://doi.org/10.1016/j.bbagen.2022.130238.

and underscores how alterations in the microenvironment rigidity regulate the proteostasis of a central Hippo pathway component.

Keywords

Hippo; MST2; Breast cells; SCF βTrCP; Extracellular matrix stiffness; Ubiquitinproteasome system

1. Introduction

The Mammalian STE20-Like Protein Kinases 1 and 2 (MST1/MST2) are part of the GCK-II subfamily of serine threonine protein kinases [1]. Early studies have shown MST1/2 involvement in apoptosis [2], and quiescence acquisition and maintenance in hepatocytes [1,3]. More recently, the discovery of “Hippo”, the Drosophila ortholog of MST1/MST2, provided evidence for novel functions for these kinases [1,4]. Hippo is the core upstream element of a tumor suppressor kinase cascade that phosphorylates and negatively regulates the transcriptional coactivator yorkie [5]. Inhibition of Hippo allows yorkie to enter the nucleus to activate the expression of pro-proliferation and anti-apoptotic genes [6]. Similar to Drosophila, the Hippo pathway in mammals relays signals from the tissue microenvironment regulating organ size [7]. Importantly, mammalian MST2, but not MST1, can rescue the phenotype caused by Hippo loss of function [4] and activate cell death [8]. Furthermore, the Hippo pathway is perturbed in several tumors and the core Hippo kinases are tumor suppressors counteracting the oncogenic activities of the Yorkie homologs, YAP (Yes-associated protein) and TAZ (transcriptional co-activator with PDZ-binding motif, also known as WWTR1) [7].

Mechanical signals from the tissue microenvironment, such as those provided by stiffness of the extracellular matrix (ECM), regulate cell shape and several cellular processes [9,10]. Cells sense composition and mechanical properties of the ECM eliciting adjustment in tension and arrangement of the actomyosin cytoskeleton [11,12]. Altered mechanical properties of the ECM are found in many diseases, including cancers [13-15]. As cancer progresses, malignant cells disturb the surrounding tissues’ physical properties [13]. Reciprocally, growing evidence has shown that tissue stiffening can induce tumorigenesis [12,13,16,17]. Commonly used for diagnosis and prognosis of several types of cancer, increased tissue stiffness is caused by ECM deposition and remodeling [13]. Although much is known regarding regulation of YAP and TAZ levels by the ECM stiffness, the mechanical influence on the Hippo pathway kinases is little understood.

We sought to investigate whether MST2 proteostasis was regulated by the proteasome. We showed that inhibition of the ubiquitin-proteasomal system led to accumulation of MST2 and that MST2 degradation was modulated by microenvironment rigidity. Furthermore, we found that MST2 interacted with the E3-ubiquitin ligase complex Skp1/Cul1/F-box-protein/β-transducing-repeat-containing protein ($SCF^{\beta TrGP}$) and that it was degraded via the proteasome. βTrCP binds to MST2 via a non-canonical degradation motif. Furthermore, activation of integrin-ILK (integrin-linked kinase) axis and the actomyosin cytoskeleton resulted in increased MST2 and βTrCP binding, leading to MST2 degradation. Our findings

shed light on the mechanisms controlling MST2-targeted proteolysis and that degradation of MST2 is a crucial part in the mechanoregulatory circuitry that senses and transduces physical cues from the cell microenvironment.

2. Results

2.1. MST2 is degraded via the proteasome upon binding to SCF$^{\beta TrCP}$

We investigated whether inhibition of the proteasome with MG132 or Cullin neddylation (a covalent conjugation of the ubiquitin-like protein NEDD8 required for activation of Cullin-dependent E3 ubiquitin ligases complexes) with MLN4924 would result in increased levels of MST2 in a panel of non-malignant and malignant human breast epithelial cell lines. Accordingly, treatment with MG132 or MLN4924 resulted in MST2 accumulation in 3 of 7 human breast cell lines grown on regular cell culture plastic plates (Fig. 1A).

To identify which specific E3-ligase complex would be responsible for ubiquitylating MST2, we assessed the literature and available interactome (BioGrid, https://thebiogrid.org/). Mass spectrometry analysis performed in our laboratory (https://massive.ucsd.edu/ProteoSAFe/dataset.jsp?accession=MSV000089341) and by others independently identified three E3-ligase substrate-recognition subunits in the MST2 interactomes: FBXO3, SKP2 and βTrCP [18-20]. All E3-ligases identified were Fbox proteins, substrate receptors that provide specificity for SCF (SKP1-Cullin1-Fbox) complexes [21]. We transfected HEK293T cells with Flag-tagged βTrCP-1 (from now on termed only βTrCP), FBXO3, or SKP2 constructs and performed immunoprecipitation (IP) assays followed by immunoblotting. Endogenous MST2 was detected only in the Flag-tagged βTrCP IP (Fig. 1B). βTrCP regulates several cellular processes targeting key regulators of cell proliferation, DNA repair and apoptosis [21-23] (Fig. 1C). Noteworthy, YAP is also targeted for degradation by SCF$^{\beta TrCP}$ [22]. Additionally, a recent report demonstrated that βTrCP binds MST2 in a precipitation assay of ectopically expressed proteins and that inhibition of the proteasome results in MST2 accumulation in HEK293T cells [23]. To confirm the direct interaction of βTrCP and MST2, we transfected HEK293T cells with a full length βTrCP or a βTrCP lacking the Fbox domain (βΔFbox), a sequence of ~40 amino acids that is required for binding to SKP1 and, hence, to assemble the SCF$^{\beta TrGP}$ complex [24]. Co-IP followed by immunoblotting revealed that MST2 binds to βΔFbox showing a more intense band than the βTrCP lane (Fig. 1D). Proteasome inhibition increased the interaction between βTrCP and MST2, but resulted in no increment of βΔFbox and MST2 binding.

This occurred, probably, because substrates bound to βΔFbox are not ubiquitylated. A ubiquitylation assay using the same constructs, βTrCP full length or βΔFbox, confirmed that only overexpression of an intact βTrCP resulted in MST2 polyubiquitylation, as assessed by Co-IP of endogenous MST2 followed by immunoblot detection of K48-Ubiquitin linkage (Fig. 1E). These co-IP experiments confirmed that MST2 interacts with βTrCP even in the absence of the intact SCF$^{\beta TrCP}$ complex, indicating that MST2 binds directly βTrCP, and not via other SCF subunits, and that βTrCP could ubiquitylate MST2.

Next, we assessed if our findings of βTrCP binding and possible regulation of MST2 levels in HEK293T cells would be consistent in a breast epithelial cell line without ectopic

overexpression. Silencing βTrCP in MCF10A cells resulted in increased levels of MST2 (Fig. 1F). The level of p21, which is not a βTrCP substrate, CUL1 and SKP1 did not change upon βTrCP knockdown.

2.2. TrCP binds to MST2 via a non-canonical degron

The Fbox protein subunits of SCFs, such as βTrCP, recognize their substrates via degradation motifs termed degrons [25]. Most known $SCF^{\beta TrGP}$ substrates contain the consensus sequence DpSGXX(*X*)pS (Fig. 2A), a biphosphorylated motif, usually localized in structurally disordered regions [26,27], that mediates the interaction of the substrate with the WD40 repeats of βTrCP. Although, MST2 does not contain a canonical βTrCP degron, we searched for sequences chemically similar to the highly conserved three amino-acid residues of the canonical degron (DpSG). Four putative tripeptide degrons are present in the human MST2 protein sequence: EDS [15-17], ESG [28-30], ESD (359–361), and EDG (375–377) (Fig. 2B). Noteworthy, similar sequences were found in other non-canonical degrons of experimentally validated $SCF^{\beta TrGP}$ targets [31-35]. We generated four Flag-tagged MST2 constructs each containing a deletion for one of the four tripeptides and transfected them into HEK293T cells for co-IP experiments using an antibody against endogenous βTrCP and detection of MST2 constructs with a Flag specific antibody. All 4 deletions affected MST2 binding to βTrCP, however deletion of the tripeptide EDG (375–377) almost abolished the interaction (Fig. 2C).

Because deletion of the MST2 EDG tripeptide produced the most prominent impairment in βTrCP interaction, we computationally modeled the MST2 segment that includes the EDG tripeptide in a complex with the βTrCP WD40 domain to investigate the structural basis that guides their recognition and interaction. The EDG tripeptide and most of its flanking residues are localized, as most degron motifs of E3-ligase targets, in a disordered region of MST2 (Suppl. Fig. 1A). In comparison to the canonical βTrCP degron motif (Fig. 2A), the first phosphorylated serine is substituted by an aspartic acid residue (D376) in MST2 EDG tripeptide, maintaining its negative charge nature (Fig. 2A). Additional glutamic acid residues N-terminal to EDG could also help provide electrostatic forces that compensate the lack of phosphorylation. The second phosphorylated serine from the canonical degron (position +4 to +5 in relation to the first phosphorylated serine) is not present in the linear sequence of MST2, and two positively charged residues occupy this position instead.

Molecular dynamics (MD) simulation of an MST2 11-mer peptide (EE**EDG**TMKRNA), starting from the position of β-catenin 11-mer peptide crystallographic structure in complex with βTrCP (see methods), showed a small deviation at the EDG tripeptide region relative to its initial position (Suppl. Fig. 1B-D).

The stability in this region is a consequence of putative hydrogen bonds between D376 in MST2 (structural position similar to pS33 from β-catenin peptide) and R285 in βTrCP as well as E375 in MST2 (structural position similar to D32 from β-catenin peptide) and R474 in β-TrCP (Fig. 2D and Suppl. Fig. 1E). In MST2, E373 also contacts R285 through hydrogen bonds. Another similarity between MST2 and β-catenin peptide binding is the presence of a hydrophobic residue (M379 of MST2 and I35 in the β-catenin peptide) pointing towards the βTrCP β-propeller channel (Fig 2D and Suppl. Fig. 1E).

During the simulation, K380 in MST2 was displaced from its initial position to avoid repulsive contact with R431 in βTrCP (Suppl. Fig. 1B), which anchors the second phosphorylated serine in canonical degrons (Suppl. Fig. 1E). The presence of βTrCP positive charges favored K380 in MST2 to be exposed to solvent. This is an interesting finding, since an *in-silico* analysis predicted K380 could be ubiquitylated (Suppl. Fig. 2A).

Protein degradation motifs are commonly conserved across species [31]. We performed interspecies alignment of MST2 and found that the MST2 EEEDGTMKRNA peptide is conserved from zebrafish to Mammalians, but it is not present in the ancestor ortholog Hippo in Drosophila (Fig. 2E).

We then assessed whether deleting the tripeptide EDG would alter MST2 susceptibility to degradation. For this, we cloned MST2-wild type (wt) or MST2-delEDG in a tetracycline inducible expression vector and transfected them into HEK293T cells. After doxycycline (Dox) treatment, both vectors showed robust protein expression (Suppl. Fig. 3). A twelve-hour pulse chase-like experiment – stimulation with Dox followed by its removal – confirmed that MST2-delEDG was indeed more resistant to degradation than the wild type protein (Fig. 2F and G). While exogenous MST2 showed an estimated half-life of ~11 h after Dox washout, MST2-delEDG estimated half-life was ~22 h. Altogether, our experimental and computational analyses revealed that MST2 can bind to βTrCP WD40 domain through the non-canonical EDG site, but maintaining structural and chemical characteristics of canonical degrons, such as the β-catenin degron.

2.3. Stiff ECM substrates and activation of integrin signaling triggers MST2 degradation

Giving the Hippo pathway key roles in mechanotransduction, we asked whether the level of MST2 was regulated by ECM stiffness. For this, we cultured MCF10A cells, a non-tumoral human mammary cell line which are highly sensitive to modulation of substrate stiffness [16], on fibronectin-coated polyacrylamide hydrogels that can be tuned in rigidity by changing the concentration of polyacrylamide [36]. Three degrees of elastic modulus were used: 0.48 KPa (Low; physiological rigidity), 4.47 KPa (Mid; average rigidity of the mammary tumor stroma) and 40.40 KPa (Hi; supraphysiological stiffness). While MST2 levels decreased in response to a stiffer ECM (Fig. 3A), we observed no changes in mRNA levels of *STK3* (gene encoding MST2) (Fig. 3B), suggesting that regulation of MST2 levels protein levels could proceed via proteolytic degradation in different mechanical contexts. Accordingly, MCF10A cells grown in high cell culture density, a condition which elicits a low tensional stress similar to a soft substrate [37], expressed higher levels of MST2 than subconfluent cell cultures [37]. In agreement with the literature [37], in high densities, inhibitory phosphorylation of YAP increased (Suppl. Fig. 4).

What pathways would mediate the signals leading to MST2 degradation in stiffer substrates? To address this question, we first confirmed that inhibition of CUL1 neddylation resulted in accumulation of MST2 in MCF10A cells cultured on stiff ECM hydrogels (Mid and Hi) (Fig. 3C). Because stiff microenvironments trigger integrin activation [12,17,38,39], we asked whether modulation of integrin signaling would result in changes of MST2 levels. We mimicked integrin hyperactivation by treating MCF10A cells with $MnCl_2$. Integrins

drastically increase affinity to their ligands when bound to Mn^{2+} [40,41]. A time-course experiment showed that MST2 levels decreased in response to Mn^{2+} (Fig. 3D).

Inhibition of CUL1 neddylation prevented the effects of integrin hyperactivation with Mn^{2+} (Fig. 3E). A 3-h treatment with Mn^{2+} (Fig. 3F) resulted in 20% reduction of MST2 levels. In addition to Mn^{2+} effects, the inhibition of protein synthesis, by co-treatment with cycloheximide (CHX), a protein synthesis inhibitor, resulted in robust MST2 decrease. We used the cell cycle inhibitor p21, a well stablished proteasome target, as a positive control for CHX treatment. Inhibition of CUL1 neddylation or proteasome activity reverted the Mn^{2+} effects on MST2 levels (Fig. 3F). To assess the direct association between integrin activation and MST2 ubiquitylation by $SCF^{\beta TrGP}$, we silenced βTrCP in combination with integrin hyperactivation by Mn^{+2}. In fact, forcing decreased levels of βTrCP abrogated the effects of integrin activation on MST2 levels (Fig. 3G).

Focal adhesions (FAs) are large protein complexes composed of kinases, FAK and/or ILK, integrins and scaffold proteins that mechanically and biochemically link the ECM to non-cytoskeleton and cytoskeleton proteins resulting in a multitude of cellular outputs [42,43]. Our hypothesis was that pharmacological perturbation of the main FA kinases (FAK and ILK) in MCF10A cells would impact MST2 proteostasis. Immunoblots for phospho-AKT and phospho-FAK confirmed that ILK and FAK were inhibited by the treatments. Surprisingly, kinetical studies showed that only ILK pharmacological inhibition resulted in higher amounts of MST2, whereas FAK inhibition did not alter the level of MST2 (Fig. 4A and B). To further verify the involvement of ILK in MST2 proteostasis, we inhibited ILK in conjunction with integrin hyperactivation by Mn^{2+}. ILK inhibition resulted in increased levels of MST2 (Fig. 4C), and decreased MST2-βTrCP binding in MCF10A cells, as assessed by Co-IP of endogenous MST2 (Fig. 4D).

Stiff substrates elevate growth factor-related pathways activated in cancer, fibrosis and other diseases [44,45]. For example, PIK3-AKT is a major growth promoting pathway that can be amplified by integrin activation. However, pharmacological inhibition of PI3K or AKT did not affect MST2 concentration (Suppl. Fig. 5A and B). Because stiff microenvironments activate actomyosin contraction, we pharmacologically inhibited myosin-II with blebbistatin, an inhibitor of myosin ATPase activity, and measured the level of MST2. MST2 levels transiently increased after myosin contraction inhibition (Fig. 4E) indicating that intracellular tension stored in the actomyosin cytoskeleton plays a role in MST2 proteostasis. This set of experiments revealed that ILK and assembly of actomyosin connect integrin activation to MST2 degradation (Fig. 4F).

3. Discussion

Besides playing crucial roles in tissue development and regeneration, Hippo kinases can be considered bona fide tumor suppressors [46]. Here, we uncovered a molecular mechanism by which MST2, one of the core Hippo kinases, degradation is regulated (Fig. 4F). We identified that $SCF^{\beta TrGP}$ binds MST2 and promotes its degradation via the 26S proteasome. In addition, we mapped the βTrCP binding motif (degron) in MST2 and described a mechano-signaling process that triggers MST2 degradation in breast epithelial cells.

Initially, we observed that levels of MST2 increased in 3 out of 7 human breast epithelial cell lines upon inhibition of the proteasome or CUL1 neddylation. Interestingly, a recent study also did not find 100% penetrance of MST2 ablation during treatment with MG132 in sarcoma cell lines [47]. This might reflect differences across the molecular background of the cells in a population. It might also suggest that in some molecular contexts MST2 is stable and/or is degraded in a proteasome-independent manner, such as autophagy-mediated degradation.

After a series of biochemical assays, using ectopic protein expression in HEK293T cells, we showed that $SCF^{\beta TrGP}$ induced MST2 degradation after binding to a non-canonical degron. Importantly, assays probing endogenous proteins in a human breast epithelial cell line confirmed these findings and also showed that ECM stiffness as well as integrin hyperactivation increased $SCF^{\beta TrGP}$ and MST2 binding, inducing MST2 degradation. We also observed that inhibition of ILK and dissipation of cytoskeleton tension built in actomyosin stress fibers caused MST2 accumulation and inhibited the interaction between $SCF^{\beta TrGP}$ and MST2. These observations revealed that MST2 is tagged for degradation by $SCF^{\beta TrGP}$ in response to activation of the Integrin-ILK axis.

The cellular microenvironment provides active and passive mechanical cues that elicit biochemical signals through the cytoskeleton and kinase cascades regulating various cellular processes such as cell proliferation [48], invasion [12], metabolism [45] and differentiation [28]. A crucial signal is the rigidity of the ECM, initially sensed by integrins that are intracellularly linked to the actomyosin cytoskeleton that in response to stiffness increase cell contractility activating mechano-sensing transcriptional activators such as YAP/TAZ [48,29]. Nevertheless, there are conflicting results in the literature as to whether the mechanical cues that influence YAP/TAZ localization and activity are mediated by Hippo kinases [30,49,50]. This observation might be attributed to the use of different cell lines, type of ECM molecule used for coating, the hydrogel preparation protocols and degrees of stiffness. Also, MST2 can phosphorylate many substrates [1] and play roles independent of its kinase activity [51]. Future studies need to address whether changes in MST2 proteostasis impact YAP/TAZ activity and have any functional consequences.

The βTrCP degron in MST2 that we identified does not contain serine - residues like the canonical degron, raising the question about how the MST2 and βTrCP interaction is regulated. But, the chemical properties of the MST2 tripeptide EDG that centers the degron are similar to the conserved DpSG in the canonical degrons and our in silico studies showed that an 11-mer MST2 peptide that includes the EDG tripeptide stably bound to βTrCP, despite the fact that the segment does not present a negative amino acid at the C-terminus that would substitute for the second phosphorylated serine in the degron. Also, deletion of other three putative tripeptide degrons MST2 resulted in decreased βTrCP and binding. Therefore, it remains to be elucidated whether phosphorylation in other regions of MST2 or other posttranslational modifications influence MST2 and βTrCP binding and if deletion of the other putative degrons has effects in protein stability. Such analyses are needed to pinpoint which molecule is linking integrin-ILK activation to regulation of MST2 and βTrCP interaction. There are, indeed, other instances in the literature of degrons that do not follow the DpSGXX(*X*)pS rule. For example, one of the WEE1 degrons (SWEEEGFGSS)

[32] and the CDH1 degron (SSPDDGNDVS) [33] do not bear the first serine found in the canonical degron. And, there is at least one report of a degron (the CDC25B degron; TEEDDGFVDI) analogous to the MST2 degron we identified, that does not contain any serine [34].

Although we clearly show that $SCF^{\beta TrCP}$ regulates MST2 proteostasis, we cannot rule out that other E3-ligases not detected in the proteomics datasets that we had access or other types of degradation (i.e. chaperone-mediated autophagy) also modulate MST2 levels. Further work will need to address this issue. Another question not addressed in the present work is if MST1 is also a $SCF^{\beta TrGP}$ target, which is possible given the similarities between MST1 and MST2 polypeptide sequences.

Tumors are frequently stiffer than normal tissues due to integrin hyperactivation [12,16,39]. We propose that engagement of integrin-ILK in the cell-to-ECM adhesion protein complexes in stiffer microenvironments could trigger MST2 degradation. This process could cooperate with other aberrant signals and reinforce malignant phenotypes in tumor microenvironments. We also suggest that the integrin-ILK-MST2 pathway might represent a novel molecular target for treating breast tumors and other types of cancers that display increased density in mammograms and low levels of Hippo activity. Based on the degron we identified, a possible strategy would be to develop peptides or small molecules that could block MST2 degradation by blunting the anchoring of βTrCP to MST2. Since MST2 bears a non-canonical βTrCP degron, targeting the βTrCP-MST2 interaction interface could reduce the chance of undesirable off-target substrates of $SCF^{\beta TrGP}$. For instance, although YAP is a substrate of $SCF^{\beta TrGP}$, its degrons differ considerably from the one we described for MST2 [22] and YAP degradation via βTrCP is activated in different mechanical contexts. While MST2 degradation is increased in stiff substrates, YAP degradation is enhanced in conditions of low mechanical stress [37]. Nevertheless, the molecular mechanisms favoring βTrCP-mediated degradation in MST2 over YAP are still elusive and need to be addressed in future studies. Finally, our work unveiled a detailed mechanism regulating MST2 levels and can have wide ramifications for the determination of cell tensional homeostasis and provide opportunities for therapeutic strategies.

4. Materials and methods

4.1. Cell lines and cell culture media

Non-tumoral breast epithelial cell lines MCF10A (Gently donated by Mina J. Bissell-Lawrence Berkeley National Laboratory) and MCF12A (Gently donated by Carlos Frederico Martins Menck, from Instituto de Ciências Biomédicas-Universidade de São Paulo) were cultured in Dulbecco Modified Eagle's/ HAM F-12 medium (1:1, DMEM/F-12, Gibco, #12-500-062), supplemented with 5% horse serum (Gibco # 16050-122), Insulin (10 μg/mL, Sigma-Aldrich, #I5500), Hydrocortisone (10 μg/mL, Sigma-Aldrich # H4001), Choleric toxin (1 μg/mL, Sigma-Aldrich, #C8052) and Epidermal Growth Factor (20 ng/mL, Sigma-Aldrich, #E4127).

Breast cancer epithelial cell lines MCF7 and MDA-MB231 (both gently donated by Mina J. Bissell – Lawrence Berkeley National Laboratory), and MDA-MB468 (purchased

from American Type Culture Collection, ATCC, #HTB-132) cell lines were cultured in DMEM high glucose (Gibco, #12100046) supplemented with 10% of fetal bovine serum (FBS, Gibco #12657-029); BT474 and SKBR3 (both purchased from ATCC #HTB-20 and #HTB-30, respectively) were cultured in RPMI (Gibco #11875093) supplemented with 10% FBS, Hyclone non-essential amino acids (0.1 mM, Thermo #SH3023801), L-glutamine (2 mM, Gibco, #25030081) and sodium pyruvate (1 mM, Gibco, #11360070). For protein level comparison in epithelial cells cultured in high and low densities, MCF10A cells were cultured, respectively, at $6.25 \times 10^4/cm^2$ and at $6.25 \times 10^3/cm^2$ for 48 h.

Human Embryonic Kidney (HEK) 293 T cells (purchased from ATCC, #CRL-11268) were cultured in Dulbecco's Modified Eagle's Medium (DMEM High Glucose, Thermo Fisher) supplemented with 10% Fetal Bovine Serum (Gibco), Hyclone non-essential amino acids (0.1 mM, Thermo), L-Glutamine (2 mM, Gibco) and sodium pyruvate (1 mM, Gibco).

4.2. Cell culture on polyacrylamide hydrogels

The polyacrylamide hydrogels with tunable mechanical properties were made in three elastic modulus levels: 0.48 kPa (3% acrylamide, 0.06% bis-acrylamide), 4.47 kPa (5% acrylamide, 0.15% bis-acrylamide) and 40.40 kPa (8% acrylamide, 0.48% bis acrylamide), as previously described [36]. The hydrogels were coated with fibronectin-1 (10 μg/mL) by using the crosslinker Sulfo-SANPAH (Pierce Biotechnology, # A35395). MCF10A cells were seeded at a density of 3×10^4 cells per cm^2 in complete medium and kept in culture for 72 h.

4.3. cDNA constructs, plasmids and transfection

All plasmids for protein expression used in this study are listed in Table S1. MST2 ORF (*STK3*, accession number NM_006281.4) was amplified from MCF10A human breast cells using specific primers (listed in Table S2) with Q5 High-Fidelity 2× Master Mix (New England BioLabs, #M0492), following the manufacturer's instructions. The MST2 ORF was inserted in the pCDNA3.1_Flag2x _Strep2x vector using StickyEnd ligase (New England Biolabs, # M0370L). The plasmids pCDNA3.1_Flag_ β-TrCP1 and pCDNA3.1_Flag_ βΔFbox were described previously [52,53]. To obtain the MST2 constructs with the tripeptide deletions, we used the pCDNA3.1_Flag2x _Strep2x _MST2 plasmid as a template, specific primers (MST2_BAMHI_Fw and MST2_XHOI_Rv, listed in Table S2) and the site directed deletions and amplification were performed using Pfu turbo DNA polymerase (Agilent, #600250) following manufacturers protocol. All constructs' sequences were confirmed by Sanger sequencing (GeneWitz, NJ) and were transfected in HEK293T cells using the Lipofectamine 3000 reagent (Thermo Fischer # L3000008).

To generate inducible vectors for MST2 wild type and del EDG we amplified the Flag2x _Strep2x fused to the MST2 constructs (wild type and del_EDG) with Q5 High-Fidelity Polymerase (New England BioLabs, # M0492) using specific primers (EcoRI_Flag_Fw and MST2_AgeI_Rv, listed in Table S2) and inserted the Flag2x _Strep2x _MST2 constructs (wild type or del_EDG) in the inducible vector pLVX (Clontech, #631847).

4.4. Gene silencing by siRNA

The following pre-designed and validated duplexes siRNA βTrCP1 (Silencer Select, Thermo #s17109) and non-targeting siRNA (AM4635) were used. Oligo duplexes were transfected using Lipofectamine RNAi-Max (ThermoFisher Scientific # 13778030) according to the manufacturer's instructions, using 200 nM of each oligo. The durations of transfection are indicated in the figures and/or figure legends.

4.5. Treatment with inhibitors and blocking peptides

Inhibitions of Cullin (CUL1) neddylation or proteasome activity were achieved by treating cells with 2.5 μM MLN4924 (Cayman Biochemicals # 15217) or 5 μM MG132 (Peptides International # IZL-3175-v) for the durations indicated in the figure legends. To assess the protein stability of MST2, we inhibited global protein synthesis with cycloheximide (CHX, 100 μg/mL, Sigma Aldrich # C4859).

Integrin activation was induced in MCF10A cells with 1 mM $MnCl_2$ (Sigma Aldrich # M1787) treatment for the durations indicated in the figure legends [54]. To screen the pathways mediating MST2 degradation, MCF10A cells were treated for 1, 3 and 6 h with the inhibitors for ILK (1 μM CPD022, Calbiochem, #407331), FAK (5 μM FAK inhibitor 14, Tocris # 3414), PI3K (30 μM LY294002, Gibco # PHZ1144), AKT (20 μM MK2206, Cayman Biochemicals #1032350-13-2) and myosin ATPase activity inhibitor (5 μM Blebbistatin, Tocris #1852).

4.6. MST2 stability assay using an inducible protein expression system

HEK293T cells were transiently transfected using Lipofectamine 3000 (ThermoFisher Scientific) based on the manufacturer's recommendation with wild type MST2 or MST2_delEDG subcloned in pLVX_TetOne-Puro (Clontech # 631849). Cells were cultured in presence of Doxycycline (Dox, 500 ng/mL Sigma Aldrich, #D9891) to induce MST2 and MST2_delEDG expression. After 24 h, Dox was washed with PBS 3 times for 30 min and complete medium was added. Cells were collected for protein extraction 3, 6, 9 and 12 h after Dox removal.

4.7. Protein extraction, immunoprecipitation, SDS-PAGE and immunoblot

For total cell lysate protein extraction, samples were lysed using modified RIPA buffer (Pierce) supplemented with protease (Sigma-Aldrich) and phosphatase inhibitors (Sigma-Aldrich). Protein concentration was determined using the DC Protein Assay kit (BioRad, #5000111). Protein lysate was resuspended at a 0.5 μg/μL concentration in Laemmli sample buffer (0.1% 2-Mercaptoethanol, 0.005% Bromophenol blue, 10% Glycerol, 2% SDS, 63 mM Tris-HCl), heated at 95°C for 5 min and kept at −20° C.

For the Co-immunoprecipitation (Co-IP) cells were lysed in immunoprecitation lysis buffer (25 mM Tris pH 8.0, 150 mM NaCl, 10% glycerol, 1 mM EDTA, 1 mM EGTA, 1 mM 1,4-Dithiothreitol (DTT) and 0.1% NP-40) containing protease (Sigma-Aldrich) and phosphatase inhibitors (Sigma-Aldrich). The insoluble fraction was removed by centrifugation (20,000 x*g* x 15 min at 4°C). Protein concentration was determined using the DC Protein Assay kit (BioRad #5000111). For both MST2 and βTrCP immunoprecipitation,

we incubated 2 mg of protein extracts with specific antibodies (listed in Table S3) overnight at 4°C. Subsequently, we added Protein A/G magnetic beads (Pierce, # 88802), incubated at 4°C for 2 h, and proceeded with extensive washing using the lysis buffer. After the final wash, the beads with the immunoprecipitant were resuspended with 1 × Laemmli sample buffer, heated at 95° C for 5 min and kept at −20°C.

The flag-tag immunoprecipitations were carried out using FLAG-M2 coated agarose beads (Sigma-Aldrich #F2426) for 2 h at 4°C. The beads were then extensively washed in lysis buffer and elution was carried out with 50 μL of 3 × FLAG peptide (Sigma-Aldrich #F4799), the supernatant was separated from the beads by centrifugation, resuspended in the same volume of 2× Laemmli sample buffer, heated at 95°C for 5 min and kept at −20°C.

Total protein extracts or immunoprecipitants were resolved in SDS-PAGE followed by immunoblot. In brief, 10 μL (5 μg) of protein sample and 20 μL of IP samples were heated at 95° C for 5 min and loaded into 10% tris-glycine polyacrylamide gels. Resolved proteins were transferred to PVDF membrane (0.45 μm, Millipore, #05317) followed by 1-h incubation in a blocking buffer (TBS, 0.5% Tween-20 with 1% BSA). Membranes were incubated in buffer (TBS, 0.5% Tween-20) containing primary antibodies (listed in Table S3) overnight, and incubated with horseradish peroxidase (HRP) for 1 h at room temperature in the blocking buffer. HRP was detected by Pierce SuperSignal detection kit (Thermo-Fisher Scientific, #A45916) and the chemiluminescence signal was captured with a ChemiDoc MP Imaging System (BioRad). All immunoblots for probing total cell lysates were performed twice.

4.8. Ubiquitylation assay

We transfected HEK293T cells with plasmids containing Flag βTrCP and Flag βTrCPΔFbox (listed in Table S1) for 24 h. Three hours prior to collection, we added 5 μM MG132, a proteasome inhibitor. Protein extraction was performed in 50 μL of buffer and under denaturing conditions (50 mM TRIS, 150 mM NaCl, 1 mM EDTA, 1% SDS) containing protease (Sigma-Aldrich #11836145001) and phosphatase inhibitors (Sigma-Aldrich #P5726-5ML) and the deubiquitylation inhibitor N-ethylmaleimide (1 μM, Sigma-Aldrich, #E3876). Samples were boiled at 98°C for 10 min and sonicated 3 times for 10 s at 4°C. Next, we added 950 μL of immunoprecipitation lysis buffer (25 mM Tris pH 8.0, 150 mM NaCl, 10% glycerol, 1 mM EDTA, 1 mM EGTA, 1 mM 1,4-Dithiothreitol (DTT) and 0.1% NP-40) containing protease (Sigma-Aldrich) and phosphatase inhibitors (Sigma-Aldrich). The insoluble fraction was removed by centrifugation (20,000 x*g* for 15 min at 4°C). We kept 100 μL of cell extract to detect MST2, Flag and β-actin as controls. For MST2 immunoprecipitation, we incubated the remaining protein extracts with polyclonal antibodies (listed in Table S3) overnight at 4°C. Subsequently, we added Protein A/G magnetic beads (Pierce, # 88802), incubated at 4°C for 2 h, and proceeded with extensive washing using the lysis buffer. After the final wash, the beads with the immu noprecipitant were resuspended with 1 × Laemmli sample buffer, heated at 95°C for 5 min and kept at −20°C.

Samples for both protein extracts or immunoprecipitants were resolved in SDS-PAGE followed by immunoblot. In brief, 10 μL of protein sample and 30 μL of immunoprecipitant

samples were heated at 95°C for 5 min and loaded into 10% tris-glycine polyacrylamide gels. Resolved proteins were transferred to PVDF membrane (0.45 μm, Millipore, #05317) followed by 1-h incubation in a blocking buffer (LiCOR Biosciences, 92760001)). Membranes were incubated in blocking buffer (LICOR) containing primary antibodies (listed in Table S3) overnight, followed by fluorescent secondary antibodies ((LiCOR Biosciences, 92532210 and 92668073) in TBS. Membranes were scanned in Odyssey CLx (LICOR).

4.9. RNA extraction, reverse transcription, and quantitative polymerase chain reaction (RT-qPCR)

Total RNA was extracted using RNeasy kit (Qiagen #74106) following the manufacturer's guidelines. The RNA 260/280 and 260/230 ratio and the concentration were measured with a Nanodrop (Thermo) UV-spectrophotometer. The cDNA was generated using 1 μg of total RNA using the kit First-Strand cDNA Synthesis (Thermo Scientific # 18080051) using oligoDT and random hexamer primers, following the manufacturer's instructions. For the qPCR, 10-μL reactions were performed in triplicates with 25 ng of cDNA using 2× SYBR Green PCR Master Mix (Applied Biosystems # 4364346) and specific primers (listed in Table S2) in MicroAmp Optical 96-Well Reaction plates (Applied Biossystems #N8010560). The reactions were performed in the AB-9500 system (Applied Biosystems) real-time thermocycler. GAPDH was used as an endogenous control and mRNA fold-changes were calculated according to the Pfaffl method [55].

4.10. Statistics

Statistical analyses and graphs were done using GraphPad Prism 7.0. The data in Figs. 2G and 3B were submitted to ANOVA followed by Dunnett test. Differences were considered significant when the *p*-value was less than 0.05.

4.11. Molecular modeling and dynamic simulation and protein sequence alignment

Human MST2 secondary structure was predicted using the PsiPred server (http://bioinf.cs.ucl.ac.uk/psipred/) [56]. An initial model of the MST2 segment that comprises EDG tripeptide (EEEDGTMKRNA) bound to β-TrCP WD40 domain was built using the main chain atoms coordinates of β-catenin peptide in a crystallographic complex with β-TrCP (PDB ID: 1P22) and changing the sidechains to match MST2 sequence. This process was performed using YASARA software (http://www.yasara.org/). Only βTrCP WD40 domain was used in modeling and simulations.

The molecular dynamic (MD) simulations were performed using YASARA with AMBER14 forcefield. For all simulations, the structures were solvated in a 10 Å cubic cell around all atoms, neutralized and submitted to energy minimization. The production runs were performed at 298 K and pH 7.4 with 2*2.5 fs timestep. All bonds and angles involving hydrogens were constrained using LINCS algorithm and an 8 Å cutoff was used for Van der Waals and Coulomb force calculation and long-range Coulomb interaction were calculated using the Particle Mesh Ewald algorithm. Simulation snapshots were saved each 250 ps. The production run of MST2 11-mer peptide EEEDGTMKRNA was performed for 200 ns and the last frame was submitted to energy minimization in YASARA and evaluated.

For MD simulations analysis, simulation snapshots were aligned using the βTrCP WD40 domain first snapshot as reference in VMD [57]. RMSD (root-mean-square deviation) and RMSF (root-mean-square fluctuation) were calculated for the MST2 peptide using the R Bio3D package [58].

For alignment of MST2 sequence from different species, we used the multi sequence alignment tool from the software Jalview 2.11.1.3 (https://www.jalview.org/).

Supplementary Material

Refer to Web version on PubMed Central for supplementary material.

Acknowledgements

This work was supported by Fundação de Amparo à Pesquisa do Estado de São Paulo (FAPESP) Young Investigator Award (14/10492-0), by a FAPESP grant (2019/26767-2), by the Conselho Nacional de Desenvolvimento Científico e Tecnológico (CNPq-Universal 444597/2014-0) and Coordenação de Aperfeiçoamento de Pessoal de Nível Superior (CAPES, Finance Code 001). MP is an investigator with the Howard Hughes Medical Institute and his lab is partially funded by grants from the National Institute of Health (R01-CA76584 and R35-GM136250). APZPF is a FAPESP Postdoctoral fellowship awardee (14/25832-1 and 17/18641-3). AMRS is funded by CAPES PhD-scholarship (PROEX), PFR is a FAPESP PhD-scholarship recipient (17/18067-5), MCSB is a FAPESP PhD-scholarship recipient (2017/25437-3) and ACM is a CNPq PhD-scholarship recipient (14668/2019-9). PLSO and HVRF are funded by a FAPESP grant (2018/00629-0). CV acknowledges funding by National Institute of Health (R35-GM127089). The authors would like to thank Dr. Gergely Róna (Department of Biochemistry and Molecular Pharmacology, New York University School of Medicine), Dr. Rebeka Tomasin (DBQ-IQUSP), Dr. Deborah Schechtman (DBQ-IQUSP), Dr. Marcelo Damário Gomes (Faculdade de Medicina de Ribeirão Preto – Universidade de São Paulo) and Dr. Hernandes F. Carvalho (UNICAMP) for all the fruitful discussions and valuable advices during the progress of this project. The authors would also like to thank Jeffrey Estrada, Celia Ludio Braga, Maria Luiza Baldini and Izaura Nobuko Toma for technical assistance.

Data availability

Data will be made available on request.

References

[1]. Galan JA, Avruch J, MST1/MST2 protein kinases: regulation and physiologic roles, Biochemistry 55 (2016) 5507–5519. [PubMed: 27618557]

[2]. Lee KK, Ohyama T, Yajima N, Tsubuki S, Yonehara S, MST, a physiological caspase substrate, highly sensitizes apoptosis both upstream and downstream of caspase activation, J. Biol. Chem 276 (2001) 19276–19285. [PubMed: 11278283]

[3]. Zhou D, et al. , Mst1 and Mst2 maintain hepatocyte quiescence and suppress hepatocellular carcinoma development through inactivation of the Yap1 oncogene, Cancer Cell 16 (2009) 425–438. [PubMed: 19878874]

[4]. Wu S, Huang J, Dong J, Pan D, Hippo encodes a Ste-20 family protein kinase that restricts cell proliferation and promotes apoptosis in conjunction with Salvador and warts, Cell 114 (2003) 445–456. [PubMed: 12941273]

[5]. Huang J, Wu S, Barrera J, Matthews K, Pan D, The hippo signaling pathway coordinately regulates cell proliferation and apoptosis by inactivating Yorkie, the Drosophila Homolog of YAP, Cell 122 (2005) 421–434. [PubMed: 16096061]

[6]. Wu S, Liu Y, Zheng Y, Dong J, Pan D, The TEAD/TEF family protein scalloped mediates transcriptional output of the hippo growth-regulatory pathway, Dev. Cell 14 (2008) 388–398. [PubMed: 18258486]

[7]. Pan D, The hippo signaling pathway in development and cancer, Dev. Cell 19 (2010) 491–505. [PubMed: 20951342]

[8]. Matsumoto H, et al. , Mammalian STE20-like kinase 2, not kinase 1, mediates photoreceptor cell death during retinal detachment, Cell Death Dis. 5 (2014) e1269. [PubMed: 24874741]

[9]. Fiore APZP, Ribeiro PF, Bruni-Cardoso A, Sleeping beauty and the microenvironment enchantment: microenvironmental regulation of the proliferation-quiescence decision in normal tissues and in cancer development, Front. Cell Dev. Biol 6 (2018) 59. [PubMed: 29930939]

[10]. Humphrey JD, Dufresne ER, Schwartz MA, Mechanotransduction and extracellular matrix homeostasis, Nat. Rev. Mol. Cell Biol 15 (2014) 802–812. [PubMed: 25355505]

[11]. Sengupta S, Rothenberg KE, Li H, Hoffman BD, Bursac N, Altering integrin engagement regulates membrane localization of K, J. Cell Sci 132 (2019).

[12]. Levental KR, et al. , Matrix crosslinking forces tumor progression by enhancing integrin signaling, Cell 139 (2009) 891–906. [PubMed: 19931152]

[13]. Nia HT, Munn LL, Jain RK, Physical traits of cancer, Science 370 (2020).

[14]. Lu P, Weaver VM, Werb Z, The extracellular matrix: a dynamic niche in cancer progression, J. Cell Biol 196 (2012) 395–406. [PubMed: 22351925]

[15]. Charras G, Sahai E, Physical influences of the extracellular environment on cell migration, Nat. Rev. Mol. Cell Biol 15 (2014) 813–824. [PubMed: 25355506]

[16]. Paszek MJ, et al. , Tensional homeostasis and the malignant phenotype, Cancer Cell 8 (2005) 241–254. [PubMed: 16169468]

[17]. Chaudhuri O, et al. , Extracellular matrix stiffness and composition jointly regulate the induction of malignant phenotypes in mammary epithelium, Nat. Mater 13 (2014) 970–978. [PubMed: 24930031]

[18]. Kim TY, et al. , Substrate trapping proteomics reveals targets of the βTrCP2/FBXW11 ubiquitin ligase, Mol. Cell. Biol 35 (2015) 167–181. [PubMed: 25332235]

[19]. Coyaud E, et al. , BioID-based identification of Skp cullin F-box (SCF)β-TrCP1/2 E3 ligase substrates, Mol. Cell. Proteomics 14 (2015) 1781–1795. [PubMed: 25900982]

[20]. Hutdin EL, et al. , Architecture of the human interactome defines protein communities and disease networks, Nature 545 (2017) 505–509. [PubMed: 28514442]

[21]. Cardozo T, Pagano M, The SCF ubiquitin ligase: insights into a molecular machine, Nat. Rev. Mol. Cell Biol 5 (2004) 739–751. [PubMed: 15340381]

[22]. Zhao B, Li L, Tumaneng K, Wang CY, Guan KL, A coordinated phosphorylation by Lats and CK1 regulates YAP stability through SCF(beta-TRCP), Genes Dev. 24 (2010) 72–85. [PubMed: 20048001]

[23]. Won GW, Park SH, Park J, Lee Y, Lee YH, Mammalian hippo kinase pathway is downregulated by BCL-2 via protein degradation, Biochem. Biophys. Res. Commun 512 (2019) 87–92. [PubMed: 30867124]

[24]. Belaïdouni N, et al. , Overexpression of human beta TrCP1 deleted of its F box induces tumorigenesis in transgenic mice, Oncogene 24 (2005) 2271–2276. [PubMed: 15735746]

[25]. Kipreos ET, Pagano M, The F-box protein family, Genome Biol. 1 (2000). REVIEWS3002.

[26]. Guharoy M, Bhowmick P, Tompa P, Design principles involving protein disorder facilitate specific substrate selection and degradation by the ubiquitin-proteasome system, J. Biol. Chem 291 (2016) 6723–6731. [PubMed: 26851277]

[27]. Low TY, et al. , A systems-wide screen identifies substrates of the SCFbetaTrCP ubiquitin ligase, Sci. Signal 7 (2014) rs8. [PubMed: 25515538]

[28]. Engler AJ, Sen S, Sweeney HL, Discher DE, Matrix elasticity directs stem cell lineage specification, Cell 126 (2006) 677–689. [PubMed: 16923388]

[29]. Wozniak MA, Modzelewska K, Kwong L, Keely PJ, Focal adhesion regulation of cell behavior, Biochim. Biophys. Acta 1692 (2004) 103–119. [PubMed: 15246682]

[30]. Dupont S, et al. , Role of YAP/TAZ in mechanotransduction, Nature 474 (2011) 179–183. [PubMed: 21654799]

[31]. Low TY, et al. , A systems-wide screen identifies substrates of the SCFβTrCP ubiquitin ligase, Sci. Signal 7 (2014) rs8. [PubMed: 25515538]

[32]. Watanabe N, et al. , M-phase kinases induce phospho-dependent ubiquitination of somatic Wee1 by SCFbeta-TrCP, Proc. Natl. Acad. Sci. U. S. A 101 (2004) 4419–4424. [PubMed: 15070733]

[33]. Fukushima H, et al. , SCF-mediated Cdh1 degradation defines a negative feedback system that coordinates cell-cycle progression, Cell Rep. 4 (2013) 803–816. [PubMed: 23972993]

[34]. Kanemori Y, Uto K, Sagata N, Beta-TrCP recognizes a previously undescribed nonphosphorylated destruction motif in Cdc25A and Cdc25B phosphatases, Proc. Natl. Acad. Sci. U. S. A 102 (2005) 6279–6284. [PubMed: 15845771]

[35]. Amir RE, Haecker H, Karin M, Ciechanover A, Mechanism of processing of the NF-kappa B2 p100 precursor: identification of the specific polyubiquitin chainanchoring lysine residue and analysis of the role of NEDD8-modification on the SCF (beta-TrCP) ubiquitin ligase, Oncogene 23 (2004) 2540–2547. [PubMed: 14676825]

[36]. Tse JR, Engler AJ, Preparation of hydrogel substrates with tunable mechanical properties, Curr. Protoc. Cell Biol 47 (2010) 10.16.1–10.16.16.. Chapter 10, Unit 10.16.

[37]. Dasgupta I, McCollum D, Control of cellular responses to mechanical cues through YAP/TAZ regulation, J. Biol. Chem 294 (2019) 17693–17706. [PubMed: 31594864]

[38]. Doornaert B, et al. , Time course of actin cytoskeleton stiffness and matrix adhesion molecules in human bronchial epithelial cell cultures, Exp. Cell Res 287 (2003) 199–208. [PubMed: 12837276]

[39]. Pang MF, et al. , Tissue stiffness and hypoxia modulate the integrin-linked kinase ILK to control breast cancer stem-like cells, Cancer Res. 76 (2016) 5277–5287. [PubMed: 27503933]

[40]. Cluzel C, et al. , The mechanisms and dynamics of (alpha)v(beta)3 integrin clustering in living cells, J. Cell Biol 171 (2005) 383–392. [PubMed: 16247034]

[41]. Lin GL, et al. , Activation of beta 1 but not beta 3 integrin increases cell traction forces, FEBS Lett. 587 (2013) 763–769. [PubMed: 23395612]

[42]. Rausch V, Hansen CG, The hippo pathway, YAP/TAZ, and the plasma membrane, Trends Cell Biol. 30 (2020) 32–48. [PubMed: 31806419]

[43]. Elad N, et al. , The role of integrin-linked kinase in the molecular architecture of focal adhesions, J. Cell Sci 126 (2013) 4099–4107. [PubMed: 23843624]

[44]. Burgstaller G, et al. , The instructive extracellular matrix of the lung: basic composition and alterations in chronic lung disease, Eur. Respir. J 50 (2017).

[45]. Park JS, et al. , Mechanical regulation of glycolysis via cytoskeleton architecture, Nature 578 (2020) 621–626. [PubMed: 32051585]

[46]. Kim NG, Koh E, Chen X, Gumbiner BM, E-cadherin mediates contact inhibition of proliferation through hippo signaling-pathway components, Proc. Natl. Acad. Sci. U. S. A 108 (2011) 11930–11935. [PubMed: 21730131]

[47]. Merritt NM, et al. , A comprehensive evaluation of hippo pathway silencing in sarcomas, Oncotarget 9 (2018) 31620–31636. [PubMed: 30167083]

[48]. Provenzano PP, Inman DR, Eliceiri KW, Keely PJ, Matrix density-induced mechanoregulation of breast cell phenotype, signaling and gene expression through a FAK-ERK linkage, Oncogene 28 (2009) 4326–4343. [PubMed: 19826415]

[49]. Seo J, Kim J, Regulation of hippo signaling by actin remodeling, BMB Rep. 51 (2018) 151–156. [PubMed: 29353600]

[50]. Alsamman S, et al. , Targeting acid ceramidase inhibits YAP/TAZ signaling to reduce fibrosis in mice, Sci. Transl. Med 12 (2020).

[51]. Chatzifrangkeskou M, et al. , RASSF1A is required for the maintenance of nuclear actin levels, EMBO J. 38 (2019) e101168. [PubMed: 31414556]

[52]. Marzio A, et al. , The F-box domain-dependent activity of EMI1 regulates PARPi sensitivity in triple-negative breast cancers, Mol. Cell 73 (2019), 224–237.e226. [PubMed: 30554948]

[53]. Guardavaccaro D, et al. , Control of meiotic and mitotic progression by the F box protein beta-Trcp1 in vivo, Dev. Cell 4 (2003) 799–812. [PubMed: 12791266]

[54]. Bazzoni G, Shih DT, Buck CA, Hemler ME, Monoclonal antibody 9EG7 defines a novel beta 1 integrin epitope induced by soluble ligand and manganese, but inhibited by calcium, J. Biol. Chem 270 (1995) 25570–25577. [PubMed: 7592728]

[55]. Pfaffl MW, A new mathematical model for relative quantification in real-time RT-PCR, Nucleic Acids Res. 29 (2001) e45. [PubMed: 11328886]

[56]. Krieger E, Vriend G, YASARA view - molecular graphics for all devices - from smartphones to workstations, Bioinformatics 30 (2014) 2981–2982. [PubMed: 24996895]

[57]. Humphrey W, Dalke A, Schulten K, VMD: visual molecular dynamics, J. Mol. Graph 14 (33–38) (1996) 27–38.

[58]. Grant BJ, Rodrigues AP, ElSawy KM, McCammon JA, Caves LS, Bio3d: an R package for the comparative analysis of protein structures, Bioinformatics 22 (2006) 2695–2696. [PubMed: 16940322]

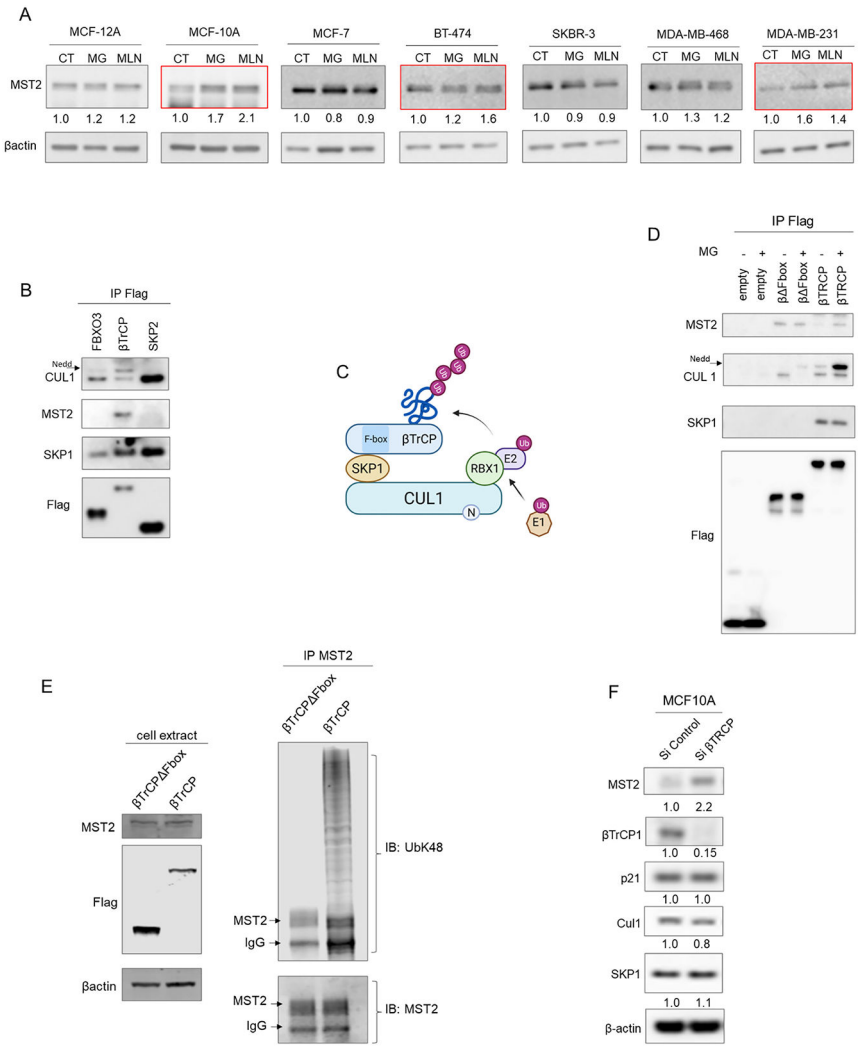

Fig. 1. MST2 is degraded via the ubiquitin-proteasome system, binds the SCF$^{\beta TrCP}$ E3 ligase and is accumulated after βTrCP silencing.

A) Immunoblots for MST2 in protein extracts from breast epithelial cell lines cultured on plastic plates in the absence (−) or presence (+) of the proteasome inhibitor MG132 (MG) or the CUL1 neddylation inhibitor MLN4924 (MN) for 3 h. Cell lines in which MST2 was accumulated upon treatments are highlighted (red outline). β-actin was used as a loading control. MST2 was considered to be accumulating when reaching at least 1.5 -fold change for at least one of the treatment conditions.

B) Co-immunoprecipitation (co-IP) FBXO3, βTrCP and SKP2 followed by immunoblotting for CUL1, MST2, SKP1 and Flag. HEK293T cells were transfected with Flag-tagged constructs FBXO3, βTrCP and SKP2. Transfected cells were treated for 1.5 h with MG, lysed and the immunoprecipitation was performed using M2 antibody coated agarose beads. Both CUL1 and SKP1 are proteins that interact with Fbox proteins and were used as Co-IP controls. Flag was detected to assess the success of precipitation of the constructs. *indicates a band that was only detected in cells transfected with wild type βTrCP.

C) Schematic of the E3 ubiquitin ligase complex SCF$^{\beta TrCP}$. As other SKP1-CUL1-Fbox (SCF) complexes, SCF$^{\beta TrCP}$ consists of 4 main subunits: SKP1, CUL1, RBX1 and the

Fbox protein βTrCP that functions as a receptor for target proteins, giving specificity to the complex. Protein degradation by the 26S proteasome depends on a cascade of enzymes. The E1 enzyme binds and activate ubiquitin (Ub), followed by the recruitment of an E2 ubiquitin-conjugating enzyme that is then loaded with activated ubiquitin. E2 interacts with the E3 complex via the adaptor protein (RBX). After a sequence of ubiquitin conjugation cycles the target protein is degraded by the proteasome. CUL1 neddylation (N) is required for SCF activation. This schematic was generated with Biorender.

D) Co-IP confirming the direct binding of MST2 and βTrCP. HEK293T cells were transfected with Flag-tag constructs fused to full length βTrCP or the dominant negative βTrCP (βΔFbox), were treated or not with MG for 1.5 h, lysed and Flag immunoprecipitation was performed using M2 antibody coated beads. Endogenous MST2, CUL1 and SKP1 (used as controls for the co-IP) and flag were detected by immunoblotting. Flag was detected to assess the success of the assay.

E) Ubiquitylation assay showing that only overexpression of βTrCP, but not βFbox, resulted in polyubiquitylation of MST2. HEK293T were transfected with Flag-βTrCP or Flag-βTrCPΔFbox and treated with MG for 3 h prior to collection. Cell extracts were submitted to co-IP of endogenous MST2. Left: Immunoblots of total cell extracts to assess the levels of the different constructs. Right: Immunoblots (IB) probing the immunoprecipitants. Polyubiquitylation was detected with a K48-linkage specific polyubiquitin antibody and MST2 was detected with the same antibody used for co-IP.

F) Silencing of βTrCP in MCF10A cells resulted in MST2 accumulation. Cells were cultured in the presence of siRNA for βTrCP or a non-targeting siRNA (si Control). Immunoblots confirmed that silencing βTrCP was efficient and resulted in increased MST2 levels. Immunoblot of p21 was used as a negative control, since it is not a βTrCP substrate. SKP1, p21 and CUL1 did not vary with βTrCP silencing. β-actin was used as loading control.

A and F) Fold changes of protein levels are shown under their respective immunoblots.

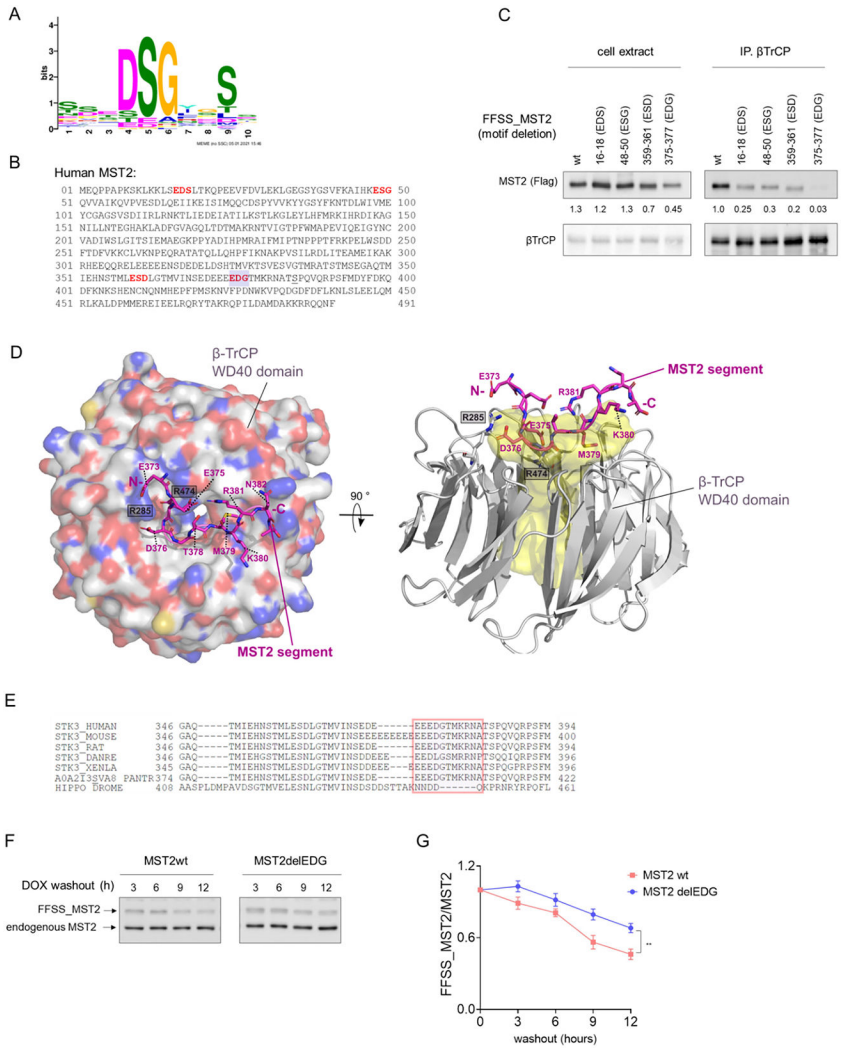

Fig. 2. βTrCP binds to MST2 via a non-canonical degron.

A) βTrCP consensus degron motif. The motif logo was generated with using MEME (http://meme-suite.org/tools/meme) according to Low et al. [13].

B) MST2 protein sequence. Four tripeptides chemically similar to DSG, the most conserved amino acid residues of the βTrCP canonical degron (Fig. 3A), are present (highlighted) in MST2 sequence: EDS [15-17], ESG [28-30], ESD (359–361) and EDG (375–377).

C) Deletion of EDG (375–377) strongly impacted MST2 interaction with βTrCP. HEK293T cells were transfected with FFSS-tagged MST2 constructs which the tripeptides identified in (B) were deleted or a wild type (wt) construct. Cells were treated with MG132 (5 μM) for 1.5 h and lysed. Endogenous βTrCP was immunoprecipitated, using a specific antibody and protein A/G-coated beads. Immunoblot for Flag was used to detect FFSS_MST2. βTrCP was detected with the same antibody used for the immunoprecipitation. Total cell extracts were also probed to assess the levels of the different constructs. Fold changes of FFSS_MST2 are shown under their respective immunoblots.

D) Structural model of the MST2 EEEDGTMKRNA peptide segment bound to βTrCP WD40 domain obtained from 200-ns MD simulation. On the left, the βTrCP WD40 domain

surface is colored by element. The MST2 peptide is presented in magenta. MST2 residues are indicated by dashed lines and β-TrCP residues are indicated in boxes. On the right, the image shows a 90° rotated view of βTrCP WD40 domain represented as cartoon and the MST2 peptide by magenta sticks. The cavity occupied by MST2 peptide is rendered as yellow surface and was determined using parKVFinder software (https://doi.org/10.1016/j.softx.2020.100606). Cavity detection was performed with the ligand adjustment mode using the following parameters: probe in of 1.4 Å, probe out of 15 Å, removal distance of 1.5 Å and ligand cutoff of 20 Å. MST2 peptide N- and C-terminals are indicated by letters.
E) Interspecies alignment of MST2 protein sequence showing that the degron sequence EDGTMKRNA is conserved from Zebra Fish to Humans. DANRE = *Danio rerio* (zebrafish); XENLA = *Xenopus laevis* (African clawed frog); PANTR = *Pan troglodytes* (chimpanzee); and DROME = *Drosophila melanogaster* (fruit fly).
F) MST2 with deleted EDG (375–377), MST2-delEDG, was more resistant to degradation than the wild type MST2 (MST2wt). HEK293T cells were transfected with FFSS-tagged MST2wt or MST2-delEDG constructs and treated for 24 h with doxycycline (Dox). After Dox washout, the cells were collected for protein extraction every 3 h for 12 h and submitted to immunoblotting with an antibody for MST2. Both ectopic and endogenous MST2 were detected as indicated in the fig.
G) Quantification of MST2wt and MST2-delEDG after Dox washout. The intensity of FFSS-tagged MST2wt and MST2-delEDG bands was normalized to the intensity of the endogenous MST2. Data are show as mean ± SEM ($n = 2$).

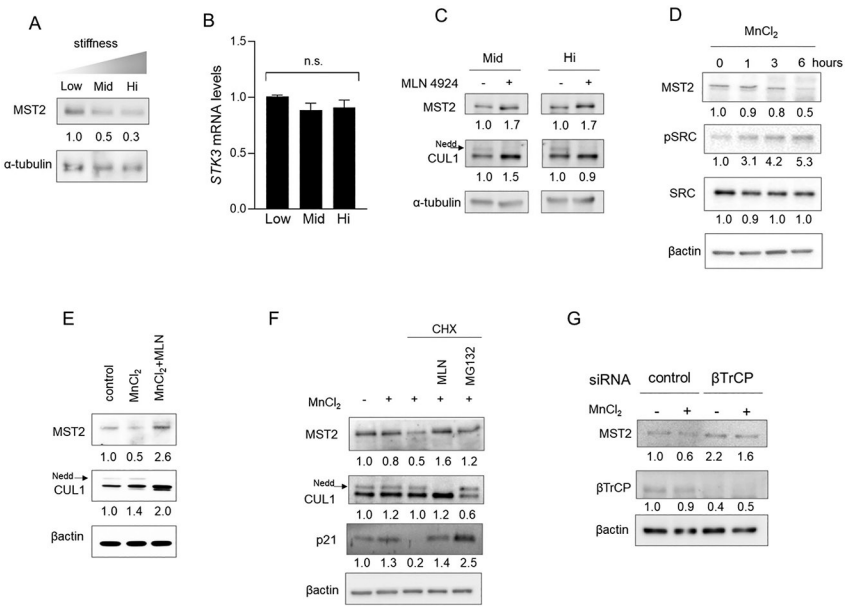

Fig. 3. ECM stiffness and integrin activation triggers MST2 degradation

A) Immunoblots for MST2 and α-tubulin (used as a loading control) of MCF10A cells cultured on fibronectin-1 (FN1) coated hydrogels with different rigidities: 0.48 KPa (Low), 4.47 KPa (Mid) and 40.40 (Hi).

B) Quantitative RT-PCR for *STK3* (gene that encodes MST2) of MCF10A cells cultured on hydrogels with different degrees of rigidity. GAPDH was used as an endogenous control to normalize gene expression. Data are expressed as mean ± SEM of $e^{\Delta\Delta ct}$ ($n = 3$).

C) Immunoblots of MCF10A cells cultured on Low and Hi rigidities and treated with CUL1 neddylation inhibitor (MLN4924). After MLN4924 (MLN) treatment, MST2 increased in both degrees of rigidity. Note that the band referring to CUL1 neddylation (indicated by an arrow) disappeared in the presence of MLN4924 indicating that the inhibition was efficient. Å-tubulin was used as loading control.

D) Immunoblots of MCF10A cells treated with $MnCl_2$ (1 mM) for 1, 3 and 6 h. SRC phosphorylation was detected to assess integrin signaling activation, β-actin was used as loading control.

E) Immunoblots of MCF10A cells pretreated with MLN for 1.5 h and then treated or not with $MnCl_2$ (1 mM) for 6 h. β-actin was used as loading control. Note that the band corresponding to neddylated CUL1 (indicated by an arrow) disappeared in the presence of MLN indicating efficient inhibition.

F) Immunoblots of MCF10A cells treated with $MnCl_2$ for 3 h, with the protein synthesis inhibitor cycloheximide (CHX) for 4 h, with MLN4294 and MG132 for 1.5 h. The different combinations of treatments are indicated in the figure panel. Note that the band referring to CUL1 neddylation (indicated by an arrow) disappeared in the presence of MLN4924 indicating that the inhibition was efficient. MST2 levels robustly decreased in the presence of $MnCl_2$ and CHX, but inhibition of the proteasome or neddylation reverses this effect. Immunoblotting for p21 was used as a positive control to assess efficiency of CHX, MLN4294 and MG132 treatments. β-actin was used as loading control.

G) Silencing of βTrCP in MCF10A cells resulted in MST2 accumulation, despite integrin signaling hyperactivation. Cells were cultured in the presence of siRNA for βTrCP or a non-targeting siRNA (siControl) and treated or not with $MnCl_2$ for 6 h. Immunoblots confirming that silencing of βTrCP was efficient and resulted in increased MST2 levels even in the presence of $MnCl_2$. β-actin was used as loading control.
(A and C-F) Fold changes of protein levels and phosphorylation of SRC (pSRC/total SRC) are shown under their respective immunoblots.

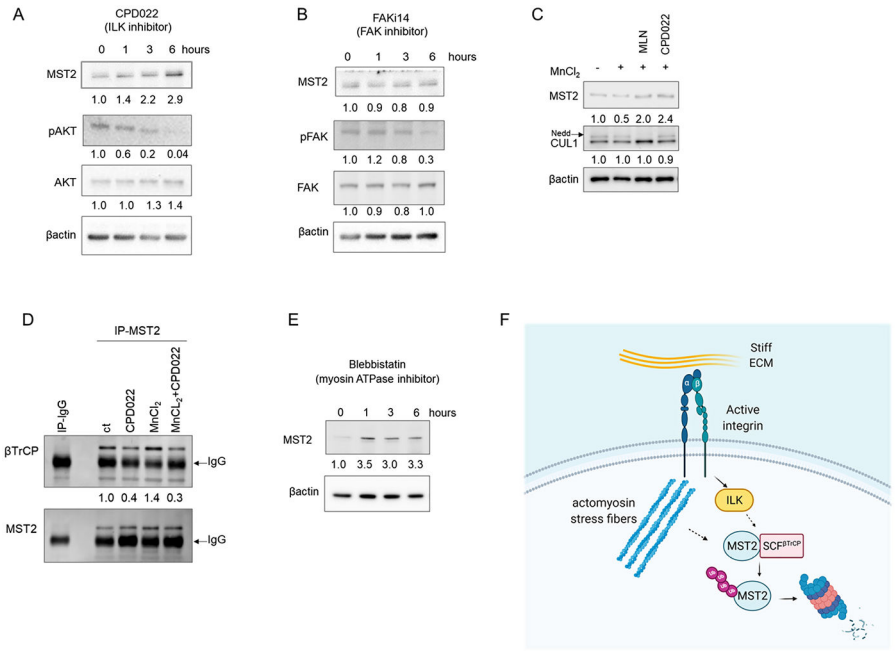

Fig. 4. Perturbation of ILK and the actomyosin cytoskeleton regulates MST2 levels:

A) Immunoblots of MCF10A cells treated with an Integrin-Linked Kinase (ILK) inhibitor (CPD022) for 1, 3 and 6 h. AKT phosphorylation was detected to assess the efficiency of ILK inhibition. β-actin was used as loading control.

B) Immunoblot for MST2 of MCF10A cells treated with FAK inhibitor (FAKi 14) for 1, 3 and 6 h. FAK phosphorylation was detected to monitor its inhibition. β-actin was used as loading control.

C) Immunoblots of MCF10A cells treated with CPD022 or MLN4294 in combination with $MnCl_2$ for 6 h. Both inhibition of CUL1 neddylation and ILK reversed the effect of integrin hyperactivation. β-actin was used as loading controls. Note that the band corresponding to CUL1 neddylation (indicated by an arrow) disappeared in the presence of MLN4924 indicating that the inhibition was efficient.

D) Co-IP revealed that the interaction of endogenous MST2 and βTrCP decreases after ILK inhibition, despite integrin hyperactivation. MCF10A cells were treated with DMSO (ct), CPD022, $MnCl_2$ or CPD022 concomitantly with $MnCl_2$ for 6 h. Co-IP was performed with an MST2 antibody or a control IgG, followed by incubation with protein A/G-coated beads. βTrCP and MST2 were only detected in the MST2 immunoprecipitants. MST2 was detected to confirm the Co-IP. Arrows indicate bands corresponding to IgG that were detected by the secondary antibody.

E) Immunoblot for MST2 of MCF10A cells treated with a myosin ATPase activity inhibitor (Blebbistatin, 2.5 μM) for 1, 3 and 6 h. β-actin was used as loading control. (A–E) Fold changes of protein levels and protein phosphorylation (phosphorylated/total) are shown under their respective immunoblots.

F) Schematic depicting the pathway of MST2 degradation induced by ECM stiffness. In a stiff ECM, hyperactive integrin signaling results in ILK activation and actomyosin

contraction leading to ubiquitylation of MST2 by $SCF^{\beta TrCP}$ and consequent MST2 degradation via proteasome 26S. This schematic was generated with Biorender.